MULTIFIDELITY RESPONSE SURFACE MODEL FOR HSCT WING BENDING MATERIAL WEIGHT

Vladimir Balabanov*

Vanderplaats Research and Development, Inc.
1767 South 8th Street, Suite M-210, Colorado Springs, CO 80906

Raphael T. Haftka†

Department of Aerospace Engineering, Mechanics and Engineering Science, University of Florida
Gainesville, Florida 32611-6250

Bernard Grossman‡, William H. Mason§, and Layne T. Watson¶

Multidisciplinary Analysis and Design (MAD) Center for Advanced Vehicles
Virginia Polytechnic Institute and State University
Blacksburg, Virginia 24061-0203

Abstract

Response surface techniques allow us to combine results from a large number of inexpensive low fidelity analyses with a small number of expensive high fidelity analyses for constructing inexpensive and accurate approximations. The paper demonstrates this approach by constructing approximations to wing bending material weight of a high speed civil transport (HSCT). The approximations employ a large number of structural optimizations of finite element models for a range of HSCT configurations. Thousands of structural optimizations of coarse finite element models are used to construct a quadratic response surface model. Then about a hundred structural optimizations of refined finite element models are used to construct linear correction response surface models. The usefulness of the approximations is demonstrated by performing aerodynamic optimizations of the HSCT while employing the response surface models to estimate wing bending material weight. The approximations for the final HSCT designs are compared to results of structural optimizations of the refined finite element model.

1. Introduction

Response surface methods have received a lot of attention in the past few years in the field of multidisciplinary optimization (MDO) [1]. These techniques construct simple algebraic approximations, typically quadratic polynomials, for the objective function and

---

* Senior Research and Development Engineer, Member AIAA
† Professor, Fellow AIAA
‡ Professor, Dept. Head, Dept. of Aerospace & Ocean Eng., Associate Fellow AIAA
§ Professor, Dept. of Aerospace & Ocean Eng., Associate Fellow AIAA
¶ Professor, Depts. of Computer Sci. and Math.

constraints, based on the values of these functions at a set of points carefully distributed throughout the design space. The optimization then proceeds on the basis of these approximations.

Response surface methods perform several important functions for MDO. They smooth out noise often present in some of the response quantities, they ease the integration of codes from various disciplines, they permit disciplinary experts to retain control over their analysis codes rather than turn them over to design optimization generalists, and they allow easy usage of parallel computer architectures (e.g., [2], [3]).

Applications of MDO, with or without response surface (RS) models, usually suffer from the high cost of the system analyses required for accurate evaluation of the objective function and constraints. Our group has pursued a variable complexity modeling approach, involving the simultaneous use of expensive high fidelity analyses together with inexpensive low fidelity analyses for alleviating this difficulty. We have used the results from the lower fidelity analyses to reduce the size of the region in design space, where the response surface model is constructed from the results from the higher fidelity analyses [3], and to reduce the number of variables in the response surface model [4] or the number of terms used [5].

In this paper we consider another approach for combining lower fidelity and higher fidelity analyses. The lower fidelity analysis is used to produce a large number of results to create a quadratic response surface model, while the expensive higher fidelity analysis is used to produce a small number of results to create a constant or linear correction factor. This approach was successfully used in the past for approximating results from structural analyses (e.g. [6, 7]). The present paper demonstrates its usefulness for approximating structural weight obtained by structural optimization of various configurations of a high speed civil transport (HSCT).

2. HSCT Design Problem

In our paper the design problem is optimization of an HSCT configuration to minimize takeoff gross weight for a range of 5500 nautical miles and a cruise Mach number of 2.4, while carrying 250 passengers. The choice of gross weight as the objective function directly incorporates both aerodynamic and structural considerations, in that the structural design directly affects aircraft empty weight and drag, while aerodynamic performance dictates the drag and thus the required fuel weight. Trim and control requirements are also explicitly treated. Figure 1 shows a typical planform of the HSCT. We have developed a simple description of the geometry and the flight trajectory that employs 29 design variables (listed in Table 1).

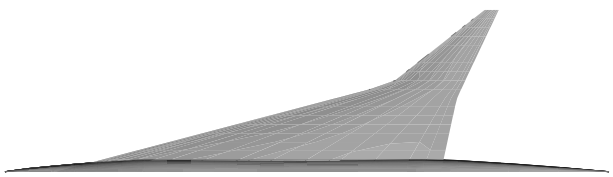

Figure 1. Typical planform of the HSCT.

Table 1. HSCT configuration design variables and baseline values.

Number	Value	Description
1	178.2	Wing root chord (ft)
2	114.1	LE break point, x (ft)
3	40.7	LE break point, y (ft)
4	173.4	TE break point, x (ft)
5	12.2	TE break point, y (ft)
6	146.4	LE wing tip, x (ft)
7	9.2	Wing tip chord (ft)
8	82.6	Wing semi-span (ft)
9	0.51	Chordwise max. t/c location
10	2.53	LE radius parameter
11	2.82	Airfoil t/c at root (%)
12	1.90	Airfoil t/c at LE break (%)
13	1.70	Airfoil t/c at tip (%)
14	2.61	Fuselage restraint 1, x (ft)
15	0.47	Fuselage restraint 1, r (ft)
16	13.24	Fuselage restraint 2, x (ft)
17	2.49	Fuselage restraint 2, r (ft)
18	111.68	Fuselage restraint 3, x (ft)
19	5.32	Fuselage restraint 3, r (ft)
20	186.91	Fuselage restraint 4, x (ft)
21	5.34	Fuselage restraint 4, r (ft)
22	11.50	Nacelle 1, y (ft)
23	28.37	Nacelle 2, y (ft)
24	464,743	Mission fuel (lbs)
25	58,403	Starting cruise altitude (ft)
26	37.97	Cruise climb rate (ft/min)
27	921.2	Vertical tail area (ft^2)
28	986.6	Horizontal tail area (ft^2)
29	57,271	Max. sea level thrust/engine, (lb)

Twenty-five of these variables describe the geometric layout of the HSCT, three variables describe the mission profile, and one variable defines engine thrust. In addition, for each planform the optimal camber distribution was obtained by the WINGDES [8] program. Sixty eight geometric, performance, and aerodynamic constraints are included in the configuration optimization process (Table 2). They are necessary to prevent the optimizer from creating physically meaningless HSCT configurations.

Weight equations (or weight functions) are usually used in the conceptual and preliminary design phases to estimate structural weight. Often, these weight equations are statistically-derived, experience based algebraic models. (See Refs. [9], [10] for a survey of wing weight equations.) We used the Flight Optimization System (FLOPS) [11] weight equation to estimate the weight of all the components of the aircraft, except for the wing bending material weight.

Table 2 Constraints on the HSCT design.

Number	Description
1	Range $\geq$ 5,500 $n.mi.$
2	Required C_L at landing speed ≤ 1
3-20	Section $C_\ell \leq 2$
21	Landing angle of attack $\leq 12^\circ$
22	Fuel volume $\leq$ half of wing volume
23	Spike prevention
24-41	Wing chord $\geq$ 7.0 $ft.$
42-43	No engine scrape at landing angle-of-attack
44-45	No engine scrape at landing angle-of-attack, with 5° roll
46	No wing tip scrape at landing
47	Rudder deflection for crosswind landing $\leq 22.5^\circ$
48	Bank angle for crosswind landing $\leq 5^\circ$
49	Takeoff rotation to occur ≤ 5 sec
50	Tail deflection for approach trim $\leq 22.5^\circ$
51	Wing root T.E. $\leq$ horiz. tail L.E.
52	Balanced field length $\leq 11,000$ ft
53	T.E. break scrape at landing with 5° roll
54	L.E. break $\leq$ semispan
55	T.E. break $\leq$ semispan
56-58	Root, break, tip $t/c \geq 1.5\%$
59	Fuselage: $x_{rest_1} \geq 5ft$
60	Fuselage: $x_{rest_1} + 10\text{ft} \leq x_{rest_2}$
61	Fuselage: $x_{rest_2} + 10\text{ft} \leq x_{rest_3}$
62	Fuselage: $x_{rest_3} + 10\text{ft} \leq x_{rest_4}$
63	Fuselage: $x_{rest_4} + 10\text{ft} \leq 300\text{ft}$
64	Nacelle 1, $y \geq$ side-of-body
65	Nacelle 1, $y \leq$ nacelle 2, y
66	Engine-out limit with vertical tail design; otherwise 50%
67-68	Maximum thrust required $\leq$ available thrust

3. Structural Optimization

Weight equations are applicable to a wide range of aircraft configurations. Because of that, weight equations may not accurately predict weights of some components of relatively new conceptual designs, such as the HSCT. In our particular case we found that wing bending material weight was not always predicted accurately enough by FLOPS.

In order to improve on the weight equation, we perform many structural optimizations in a region around a nominal configuration and create a customized weight function (quadratic RS model) which is tailored to the HSCT and its particular design requirements. This quadratic RS model was used to replace the wing bending material weight portion of the FLOPS weight equation.

Due to the large number of optimizations that must be performed to create a response surface model, a relatively coarse structural optimization model was used. We employed a structural model of the HSCT with a fixed arrangement of spars and ribs. The wing and fuselage skin were modeled by membrane elements. Spar and rib caps were modeled by rod elements. Vertical rods and shear panels were used to model spar and rib webs. Because of symmetry, we only generated a finite element (FE) model of half the aircraft. Our typical coarse FE model of the HSCT consisted of $1,127$ elements joined together at 226 nodes with a total number of $1,242$ degrees of freedom (Figure 2). Forty design variables were used in the coarse FE model, including 26 to define skin panel thicknesses, 12 for spar cap areas, and two design variables for the rib cap areas. Within each group a uniform thickness or area distribution was assumed.

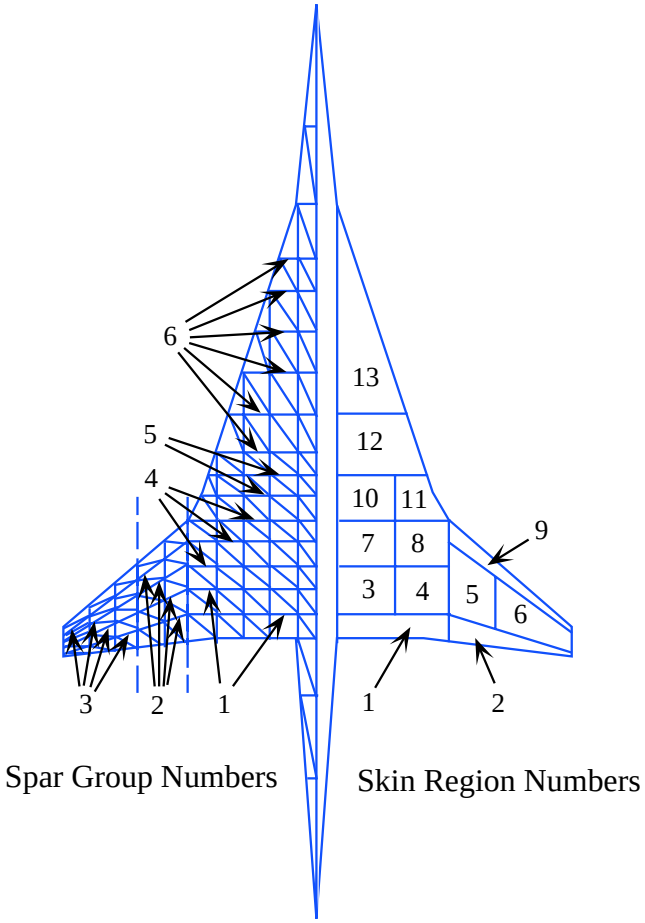

Figure 2. Coarse HSCT FE model and structural design variables.

We applied stress constraints based on the Von Mises yield criterion to each panel, spar, and rib cap element. In addition, local buckling constraints were applied. We only employed the results of the structural optimization to estimate the bending material weight of the structure, and continued to use FLOPS weight equation to estimate other parts of the structural and nonstructural weight. Following the FLOPS weight equation breakdown, the bending material weight was defined to consist mostly of the weight of the spar caps and skin panels. It accounted for about 4.5% of the gross takeoff weight. However, the

entire wing structural weight was the objective function of the structural optimization. After optimization was performed, wing bending material weight was calculated based on the thickness of specific portions of the wing.

The loads applied to the structural model were composed of aerodynamic and inertia forces. Inertia loads represented the combined effects of non-structural items, fuel weight, and the distributed weight of the structure. Aerodynamic loads for supersonic flight conditions were determined using a supersonic panel method, and loads for subsonic flight conditions were from a vortex-lattice method. The structure was assumed to be rigid for the determination of aerodynamic forces. Previous studies indicated that structural flexibility did not have a large effect on the structural wing weight (objective function of the structural optimization) for this particular configuration [12, 13]. A surface spline interpolation method was used to translate forces between aerodynamic node and structural node locations. Five load cases were considered for the structural optimization (Table 3). More details about loads can be found in Refs. 14, 15.

Table 3. Load cases for the structural optimization.

Load case	**Mach number**	**Load factor**	**Altitude (ft.)**	**% of fuel**
High-speed cruise	2.4	1.0	63175	50
Transonic climb	1.2	1.0	29670	90
Low-speed pull-up	0.6	2.5	10000	95
High-speed pull-up	2.4	2.5	56949	80
Taxiing	0.0	1.5	0	100

A finite-element-based structural optimization code GENESIS [16], was used to optimize the HSCT configurations. The large number of structural optimizations required made this problem especially suitable for coarse grain parallelization. The structural optimization required about 40 minutes each when performed on a single node. Instead, we performed the optimizations on $30 - 50$ nodes at a time, with an average efficiency of about 0.6, so that we could perform about 30 structural optimizations per hour. A coarse-grain parallelization of GENESIS on the Intel *Paragon* greatly accelerated the creation of the response surface models.

Initially we only used a coarse FE model that was optimized thousands of times to create the weight equation [14]. Next we created a more refined, higher fidelity, finite element model of the HSCT wing structure. The refined FE model had a larger number of design variables than the coarse FE model — 74. Figure 3 shows an example of such a FE model. It had $2,214$ elements, 555 nodes, and $3,216$ degrees of freedom. That model also included the landing gear bay, missing from the coarser model. Comparison of the the optimal structural weight for the two models for a few aerodynamic configurations revealed substantial differences. Consequently, we sought to correct the quadratic RS model created from the results of the structural optimizations with the coarse FE model. One structural optimization for the refined FE model required about 4 hours on a single node of the Intel *Paragon*. We could afford a relatively small number of structural optimizations with the refined FE model. Consequently, the correction must be of lower order, that is, constant or linear.

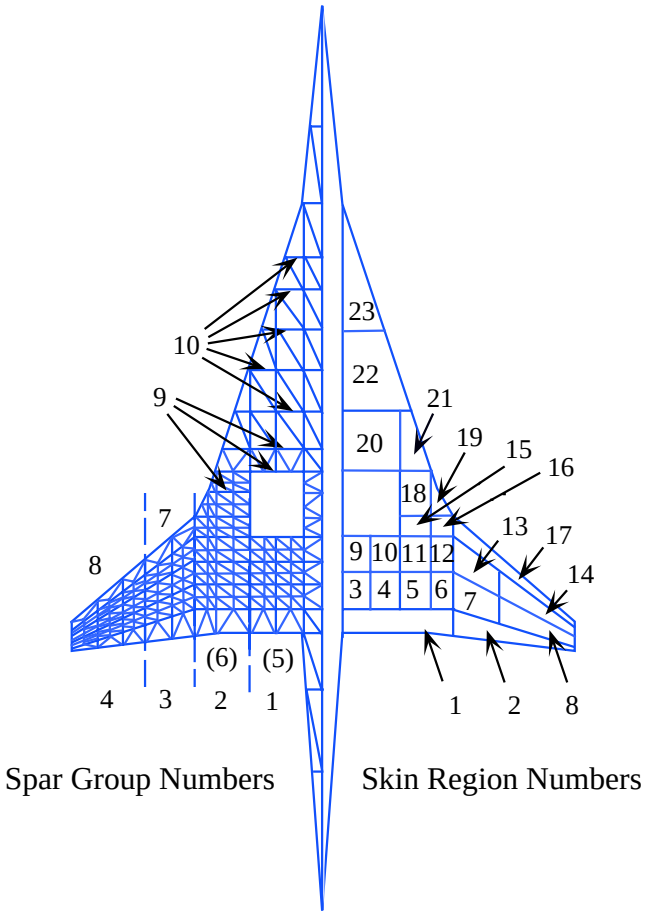

Figure 3. Refined HSCT FE model and structural design variables.

3.1 Noise in the Structural Optimization Results

The weight obtained by structural optimization is not a smooth function of the configuration design variables. This nonsmoothness is the result of changes in the set of active constraints as the configuration changes and numerical noise which includes incomplete convergence of the structural optimization as well as noise in the aerodynamic loads.

A procedure which we use to detect noise in a response quantity is to plot the response along a straight line segment in design space. This plot is sometimes called an α plot. The segment is obtained by connecting two close design points:

$$\mathbf{x} = (1-\alpha)\mathbf{x_s} + \alpha\mathbf{x_f} \ , \quad 0 \le \alpha \le 1$$

where $\mathbf{x_s}$ is the vector of starting design variables, $\mathbf{x_f}$ is the vector of final design variables.

In order to check the amount of noise in the results of the structural optimization for the coarse FE model, two close, conventionally looking HSCT designs are chosen as the endpoints of the segment. These designs are referred to as Design #1 and Design #20 (shown in the Figure 4).

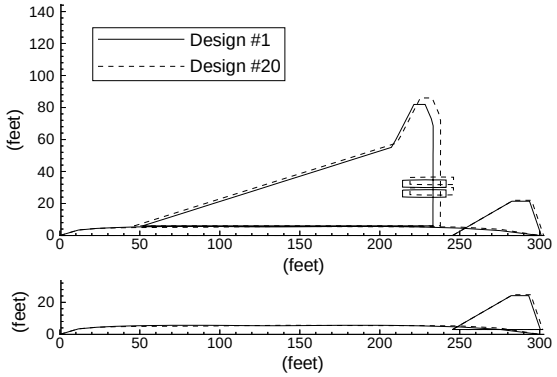

Figure 4. First and last designs in α plot

The configuration design variables which define these two designs differ by about 3%. Eighteen additional equally spaced designs are taken along the straight line segment connecting two endpoint designs.

Figure 5 shows the variation in the wing bending material weight from structural optimization of the coarse FE model for the 20 designs. It appears from the figure that the noise in the structural optimization weight is on the order of $5 - -10\%$. Note, that the FLOPS estimate is also presented in the figure.

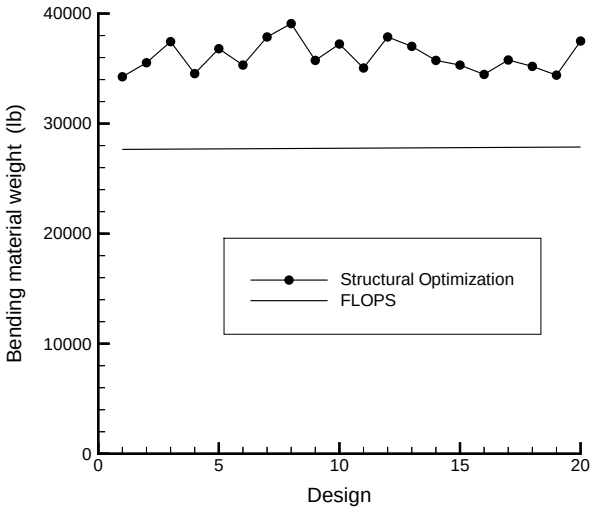

Figure 5. Noise in wing bending material weight.

4. Construction of Response Surface Models

We performed structural optimization with the coarse FE model for $2,107$ HSCT configurations. The set of points S_q corresponding to these configurations form a small composite design (SCD) in 29 design variables. Consider the p-dimensional box centered at the origin of the system of coordinates. Then SCD represents a fraction $(2^{(p-m)})$ of vertices of this

box, point at the center, and $2p$ points at the axis of the system of coordinates, located symmetrically with respect to the center of the box. We used $2^{(29-18)}$ fraction of the vertices for our particular case. The points for SCD were generated using the program SAS [17]. More details about SCD can be found in Ref. 18, pp. 351–355.

We constructed a quadratic response surface model from the results of the structural optimization at the set S_q of $2,107$ points. A full quadratic RS model in 29 variables has 465 terms. We used two approaches to eliminate poorly defined terms in the response surface model: the backward elimination procedure and the stepwise regression procedure followed by backward elimination ([18], pp. 650–655). The same model was obtained using both approaches. It was possible to estimate 96 terms in the response surface model with a p-value ([18], pp. 31–38) less or equal to 0.05. The unbiased root mean square error estimate for this model was about 4.1%.

We selected a subset S_l of 101 D-optimal ([18], pp. 364–366) points from the set S_q of 2107 points to construct linear correction RS models. Another set of 100 points S_t was randomly selected from S_q to test the performance of the linear correction RS models at a set of points different from the set of points used to create the correction RS models. This number of points (100) is approximately three times the number of coefficients in the linear correction RS models.

Refined structural optimizations were performed for S_l and S_t. The differences between the wing bending material weight calculated by the coarse structural optimization and by the refined structural optimization for the two sets of points S_l and S_t are summarized in Table 4. The average value of the wing bending material weight from the refined structural optimization was about $55,000$ lb for both S_l and S_t. From Table 4 we see that on average the refined structural optimization predicts 25% heavier wing bending material weight than the coarse structural optimization.

Table 4. Differences in wing bending material weight from coarse (B_c) and refined (B_r) structural optimizations at two sets of points: S_l and S_t.
Average value of B_r is 55,000 lb for both S_l and S_t.

Parameter	**Min**	**Average**	**Median**	**Max**	**Std Dev**
B_r - B_c at S_l	-5,253 lb	10,813 lb	10,382 lb	29,572 lb	5,285 lb
B_r - B_c at S_t	-5,253 lb	11,364 lb	11,867 lb	25,818 lb	4,915 lb
B_c / B_r at S_l	0.5904	0.8047	0.8073	1.073	0.08833
B_c / B_r at S_t	0.6516	0.7944	0.7795	1.073	0.08560

We evaluated the errors of the coarse RS model with respect to the refined structural optimization results at S_l and S_t (Table 5). The average, median, and maximum values of the error of the RS model agree well with the differences between the refined and the coarse structural optimization results (Table 4), which indicates that there is not much difference between a comparison of the actual data and the values from the RS model.

Table 5. Errors in the coarse RS model at two sets of points with respect to the results of the refined structural optimization. Here RMSE is the root mean square error.

Set of points	**RMSE**	**Average**	**Median**	**Maximum**	**Std. Dev.**
S_l	11,880 lb	10,685 lb	10,279 lb	28,463 lb	5,220 lb
S_t	12,356 lb	11,409 lb	11,252 lb	23,620 lb	4,768 lb

We used several approaches for correcting the RS model based on the coarse FE model. To describe these approaches we introduce the following notation:

d_a – average difference between the results of refined and coarse structural optimizations at S_l $(10,813\ lb)$;

r_a – average ratio of the results of coarse structural optimizations to the results of refined structural optimizations at S_l (0.8047);

B_c – bending material weight from coarse structural optimizations at S_q $(2,107$ points);

B_c^{corr} – corrected bending material weight at S_q;

$RS1$ – response surface model constructed from the coarse structural optimizations, B_c;

RS_{ac} – linear additive correction response surface model (constructed at S_l);

RS_{mc} – linear multiplicative correction RS model (constructed at S_l);

RS^{corr} – corrected quadratic RS model.

We used the correction response surface models to correct either the results of the quadratic RS model constructed from the coarse structural optimizations results ($RS1$), or to correct the data used for construction of the quadratic RS model. Using the notation above, these approaches can be summarized as follows:

(i_a) $\quad RS^{corr} = RS1 + d_a$;

(ii_a) $\quad RS^{corr} = RS1 + RS_{ac}$.

(iii_a) and (iv_a) are similar to (i_a) and (ii_a), but coarse data is corrected instead of coarse RS models:

(iii_a) $\quad B_c^{corr} = B_c + d_a$;

(iv_a) $\quad B_c^{corr} = B_c + RS_{ac}$.

When (iii_a) or (iv_a) are completed, RS^{corr} is obtained by passing a new RS model at the corrected data points. In fact, approaches (i_a) and (iii_a) are identical, because (iii_a) results in shifting all the data by the same amount, thus, preserving all the features of $RS1$, except for the constant term. As the shift in (i_a) and (iii_a) is the same, the predicted weights are also the same for RS^{corr} from (i_a) and for RS^{corr} created from B_c^{corr} of (iii_a).

Four analogous multiplicative corrections were also introduced, as:

(i_b) $\quad RS^{corr} = RS1/r_a$;

(ii_b) $\quad RS^{corr} = RS1/RS_{mc}$;

(iii_b) $\quad B_c^{corr} = B_c/r_a$;

(iv_b) $\quad B_c^{corr} = B_c/RS_{mc}$.

To eliminate poorly defined terms in the linear correction RS models we again used two different approaches: the backward elimination procedure and the stepwise regression procedure followed by backward elimination. For the threshold p-value of 0.05 it was possible to estimate only four out of the original 30 terms for the additive RS model, RS_{ac}, and nine out of 30 terms for the multiplicative RS model, RS_{mc}.

5. Accuracy of Correction RS Models

The errors in the wing bending material weight approximations using the additive and multiplicative RS models are summarized in Figures 6 and 7 versus the number of terms retained in the models. Note that the values in Figure 6 for one term, correspond to case (i_a). The errors with the four term additive correction and the nine term multiplicative correction are summarized in Table 6.

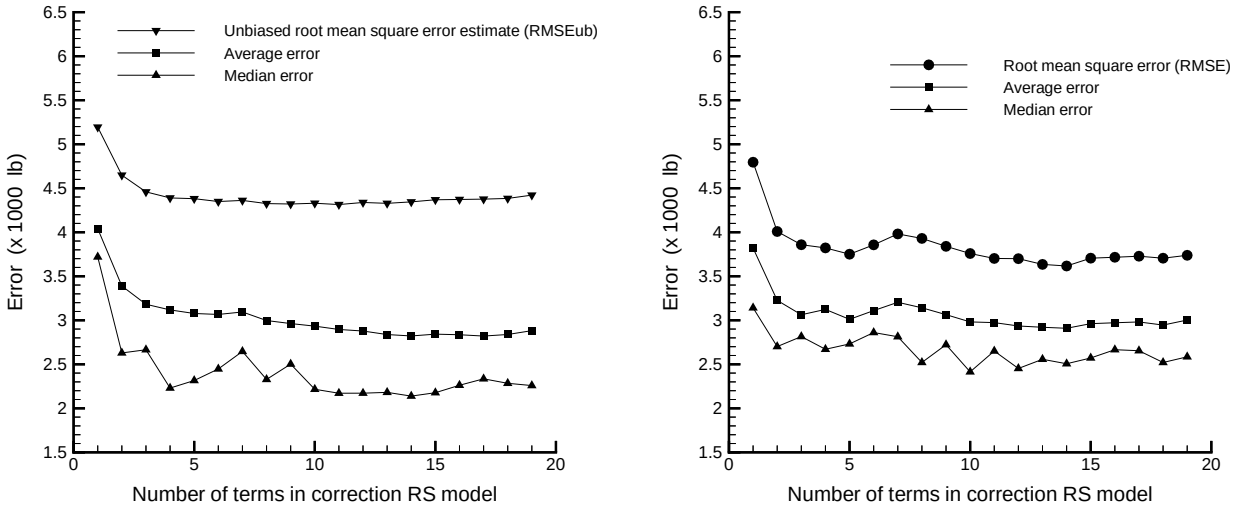

(a) (b)

Figure 6. Errors at S_l (a) and S_t (b) with additive correction to RS models. Cases (i_a) and (ii_a).

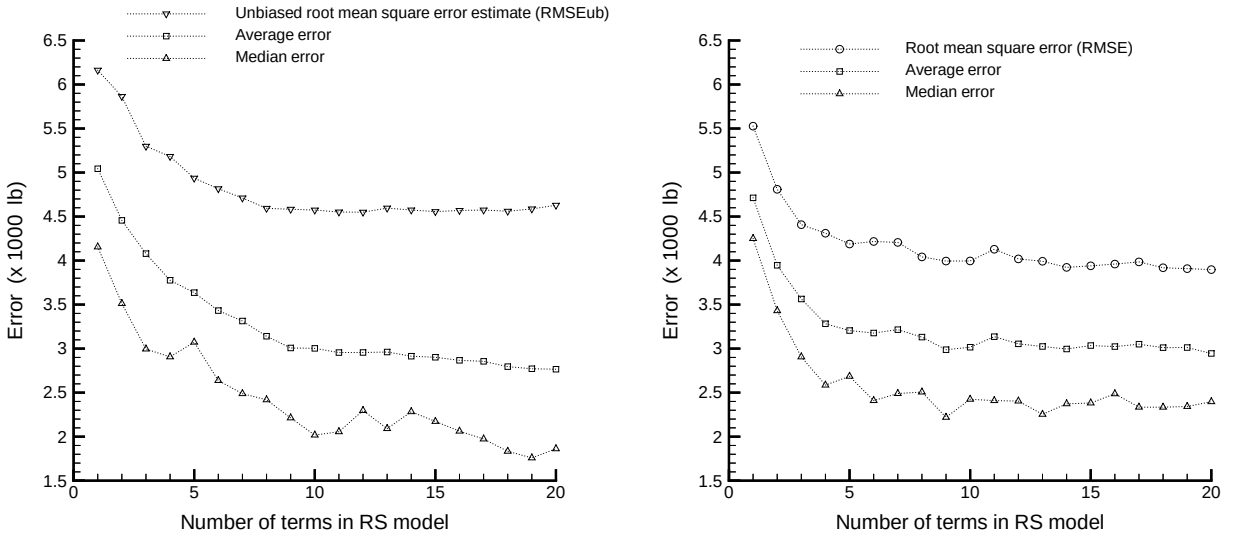

(a) (b)

Figure 7. Errors at S_l (a) and S_t (b) with multiplicative correction to RS models. Cases (i_b) and (ii_b).

Table 6. Errors of the corrected quadratic RS models at two sets of points with respect to the results of the refined structural optimization. Here RMSE is the root mean square error.

RS and Set	RMSE	Average	Median	Maximum	Std. Dev.
$RS1_{ac}^{corr}$ at S_l	4,324 lb	3,118 lb	2,230 lb	17,540 lb	3,011 lb
$RS1_{ac}^{corr}$ at S_t	3,822 lb	3,123 lb	2,670 lb	9,830 lb	2,214 lb
$RS1_{mc}^{corr}$ at S_l	4,422 lb	3,072 lb	2,240 lb	18,747 lb	3,196 lb
$RS1_{mc}^{corr}$ at S_t	3,992 lb	3,051 lb	2,292 lb	12,723 lb	2,587 lb

The results in Figures 6 and 7 and in Tables 5 and 6 indicate that the error of the coarse RS model can be reduced by more than 50% by using the constant correction, d_a (Case (i_a)) or r_a (Case (i_b)). The few additional terms in the linear correction RS models improve the accuracy just a little more. It is also possible to conclude that on average the linear additive correction RS model is slightly better than the linear multiplicative correction RS model.

To separate the errors associated with the coarse RS model from the errors of the linear correction RS models, we recalculated the errors without using the coarse RS model, but instead correcting all $2,107$ coarse data points (data B_c at the set of points S_q). We used approaches (iv_a) and (iv_b) described above, that is, passing a RS model through the corrected data. The results obtained were close to the corresponding results from Figures 6 and 7. From that we may conclude that for our case there is not much difference in approaches (ii_a) and (iv_a) or in approaches (ii_b) and (iv_b), i.e., it does not matter much if we correct the results of the coarse RS model or we correct the data B_c and recreate the quadratic RS model from the corrected data.

6. HSCT Configuration Optimization employing Correction RS Models

HSCT configuration optimizations were performed to evaluate the effects of using the correction RS models. Several different approaches were tried for estimating wing bending material weight within the configuration optimization:
(1) FLOPS weight equation.
(2) $RS1$: RS model from the results of the coarse structural optimization.
(3) $(RS1 + d_a)$: Coarse RS model, $RS1$, corrected by the average difference, d_a.
(4) $RS1_{ac}^{corr}$: $RS1$ corrected by the additive correction RS model.
(5) $RS1_{mc}^{corr}$: $RS1$ corrected by the multiplicative correction RS model.

Each configuration optimization was started from the baseline HSCT configuration. Some parameters of the obtained optimal HSCT configurations are given in Table 7. The gross take off weight presented in this table was calculated using the approximate bending material weight employed in the corresponding configuration optimization. The planforms of the aircraft are plotted in Figure 8.

Table 7. Parameters of optimal HSCT configurations obtained with various wing bending material weight approximations. Optimizations started from the baseline HSCT configuration. Notation:
B_{FLOPS} – bending material weight by FLOPS;
B_{RS1} – bending material weight by $RS1$;
B_c – bending material weight by coarse structural optimization;
$B_{RS1_{d_a}}$ – bending material weight by $RS1$ corrected with d_a;
$B_{RS1_{ac}}$ – bending material weight by $RS1^{corr}_{ac}$;
$B_{RS1_{mc}}$ – bending material weight by $RS1^{corr}_{mc}$;
B_r – bending material weight by refined structural optimization.
An asterisk denotes weight used in the optimization.

FLOPS	**RS1**	**RS1 + $\mathbf{d}_a$**	**RS1$^{corr}_{ac}$**	**RS1$^{corr}_{mc}$**	**Parameter**
			Planform Geometrty		
180.2	180.4	169.1	163.4	162.8	Wing root chord (ft)
10.3	10.3	9.5	10.0	10.0	Wing tip chord (ft)
72.9	72.4	74.7	76.7	77.1	Wing semi-span (ft)
1.89	1.80	1.85	1.98	2.03	Aspect Ratio
13,214	13,637	14,086	13,828	13,607	Wing Area (ft^2)
2.59	2.74	2.84	2.74	2.82	Root t/c (%)
			Performance Data		
5,501	5,500	5,487	5,497	5,501	Range $(n.\ mi.)$
9.01	9.00	8.97	8.98	9.00	L/D_{max} at $M = 2.4$
			Weight Data		
420,336	422,480	453,687	459,980	456,730	Required Fuel Weight (lb)
$27,491^*$	27,909	39,590	45,455	46,630	B_{FLOPS} (lb)
33,359	$22,990^*$	37,202	43,088	46,566	B_{RS1} (lb)
33,823	28,319	37,611	45,721	49,000	B_c (lb)
44,067	33,697	$47,910^*$	53,796	57,274	$B_{RS1_{d_a}}$ (lb)
41,777	35,148	47,596	$51,616^*$	54,784	$B_{RS1_{ac}}$ (lb)
42,458	34,773	47,026	51,638	$52,888^*$	$B_{RS1_{mc}}$ (lb)
36,954	37,280	51,260	50,315	57,846	B_r (lb)
797,529	797,167	859,019	872,653	868,503	Gross Take Off Weight (lb)

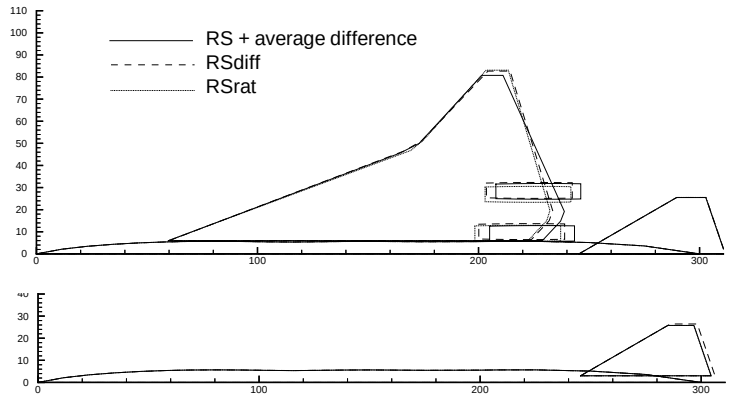

Figure 8. Optimal HSCT configurations employing correction RS models. Optimizations were started from the baseline HSCT configuration. Here (*RS + average difference*) denotes using $(RS1 + d_a)$; *RSdiff* denotes using $RS1_{ac}^{corr}$; *RSrat* denotes using $RS1_{mc}^{corr}$.

From Table 7 we note that the errors at the optimal design are somewhat larger than the average errors in Tables 5 and 6, and that they tend to be unconservative. $RS1_{ac}^{corr}$ is an exception on both counts, but this may be a matter of chance. This tendency indicates that the optimization procedure capitalizes on weaknesses in the RS models.

From Table 7 and Figure 8 we see that when the corrected RS models $RS1_{ac}^{corr}$ and $RS1_{mc}^{corr}$ were used, the configuration optimization converged to very similar designs. The configuration obtained using the average difference correction looks slightly different from the configurations obtained using $RS1_{ac}^{corr}$ and $RS1_{mc}^{corr}$. The gross take off weights obtained for the three optimum designs are comparable. The gross take off weight is lower for the design obtained using the average difference correction. However, if we correct the error in the wing bending material weight for this configuration and add the fuel needed to carry the additional weight, the gross take off weight for this configuration will be much closer to the one obtained with $RS1_{ac}^{corr}$.

We also performed HSCT configuration optimization starting from the optimal configuration obtained using FLOPS. Some parameters of the obtained optimal HSCT configurations are given in Table 8. The gross take off weight presented in this table was calculated using the approximate bending material weight employed in the corresponding configuration optimization. The planforms of the aircraft are plotted in Figure 9.

Table 8. Parameters of optimal HSCT configurations obtained with various wing bending material weight approximations. Optimizations started from the FLOPS optimum. Notation:
B_{FLOPS} – bending material weight by FLOPS;
B_{RS1} – bending material weight by $RS1$;
B_c – bending material weight by coarse structural optimization;
$B_{RS1_{d_a}}$ – bending material weight by $RS1$ corrected with d_a;
$B_{RS1_{ac}}$ – bending material weight by $RS1^{corr}_{ac}$;
$B_{RS1_{mc}}$ – bending material weight by $RS1^{corr}_{mc}$;
B_r – bending material weight by refined structural optimization.
An asterisk denotes weight used in the optimization.

RS1	**RS1 + $\mathbf{d}_a$**	**RS1$^{corr}_{ac}$**	**RS1$^{corr}_{mc}$**	**Parameter**
		Planform Geometrty		
180.4	180.1	180.5	180.5	Wing root chord (ft)
10.3	10.1	10.2	10.2	Wing tip chord (ft)
72.4	74.8	75.8	75.8	Wing semi-span (ft)
1.81	1.83	1.89	1.86	Aspect Ratio
13,559	14,296	14,181	14,378	Wing Area (ft^2)
2.73	2.76	2.71	2.79	Root t/c (%)
		Performance Data		
5,499	5,496	5,503	5,501	Range $(n.\ mi.)$
8.98	8.96	8.94	8.96	L/D_{max} at $M = 2.4$
		Weight Data		
423,815	458,481	458,926	459,085	Required Fuel Weight (lb)
26,860	34,349	30,381	34,862	B_{FLOPS} (lb)
$23,512^*$	28,517	29,557	29,828	B_{RS1} (lb)
28,644	33,045	32,599	34,203	B_c (lb)
34,220	$39,225^*$	40,265	40,536	$B_{RS1_{d_a}}$ (lb)
34,917	40,424	$39,063^*$	41,659	$B_{RS1_{ac}}$ (lb)
34,868	39,309	38,810	$38,790^*$	$B_{RS1_{mc}}$ (lb)
38,099	43,231	42,337	46,933	B_r (lb)
798,693	868,261	868,132	869,566	Gross Take Off Weight (lb)

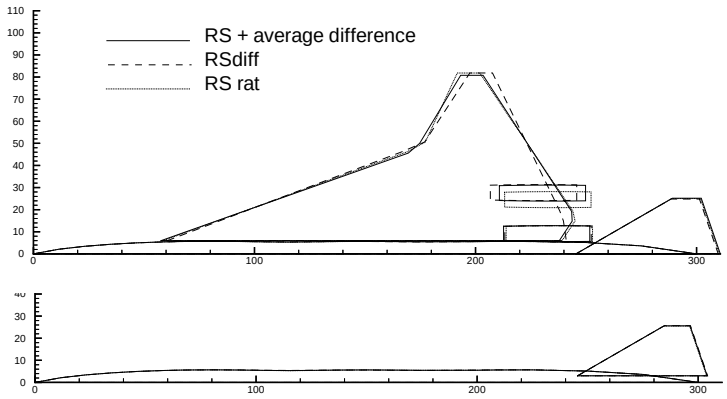

Figure 9. Optimal HSCT configurations employing correction RS models.
Optimizations were started from the FLOPS optimum.
Here (*RS + average difference*) denotes using $(RS1 + d_a)$;
RSdiff denotes using $RS1_{ac}^{corr}$;
RSrat denotes using $RS1_{mc}^{corr}$.

Though the optimal configurations obtained are different from the ones when optimization was started from the baseline configuration, the gross take off weights of the aircraft are comparable.

From Tables 7 and 8 we find that the additive correction is consistently more accurate at the optimum than the multiplicative correction or the correction by the average. However, this may be an idiosyncrasy of the example. The error of $RS1$ (based on the coarse FE model) at the optimum is of the order of 40%, while the errors associated with the various correction response surfaces range from 2.5% to 17.3%.

Convergence to different HSCT configurations when starting from different initial points may reflect the nonconvexity of the design domain. In addition the aerodynamic constraints used in the configuration optimization have numerical noise in them [19]. Thus several local optima are very likely to exist.

7. Concluding Remarks

The paper demonstrated the use of response surface techniques for combining a large number of inexpensive low fidelity results with a small number of expensive high fidelity results. A large number of structural optimizations based on the coarse finite element model were combined with a small number of optimizations based on the refined model for constructing approximations to wing bending material weight in terms of configuration design variables of an HSCT. Quadratic models were fit to coarse model results, and linear models were used as additive or multiplicative corrections. The accuracy of the approximations was tested at a randomly chosen set of 100 points as well as by using the approximations for configuration optimization and checking their accuracy at the optima. It was found that:

1. The linear correction response surfaces reduced the errors of the quadratic response surfaces based on coarse models by more than half.
2. Most of the reduction was obtained even with a constant correction, with the linear terms adding only marginal improvements.
3. The additive correction performed slightly better at the test data points, and substantially better for the optimal designs.
4. It did not matter if the correction response surface was applied to the coarse model data followed by fitting a new quadratic surface or if the original quadratic response surface was corrected directly.

Acknowledgement

This work was supported by NASA Grants NAG-1-1562 and NAG-1-1160.

References

1. Sobieszczanski-Sobieski, J. and Haftka, R. T., "Multidisciplinary Aerospace Design Optimization: Survey of Recent Developments," *Structural Optimization*, 14(1), pp. 1–23, 1997.
2. Oakley, D., Sues, R. H., and Rhodes, G. S., "Multilevel Parallel Computing for Multidisciplinary Optimization and Probabilistic Mechanics", Proceedings of the *37th AIAA/ASME/ASCE/AHS/ASC Structures, Structural Dynamics, and Materials Conference and Exhibit*, Salt Lake City, UT, April 15–17, 1996, pp. 620–628, AIAA 96–1387–CP.
3. Giunta, A. A., Balabanov, V., Burgee, S., Grossman, B., Haftka, R. T., Mason, W. H., and Watson, L. T., "Variable-Complexity Multidisciplinary Design Optimization Using Parallel Computers", *Computational Mechanics'95 – Theory and Applications*, pp. 489–494, 1995. Editors: Alturi, S. N., Yagawa, G., Cruse, T. A., Springer, Berlin.
4. Kaufman, M., Balabanov, V., Burgee, S. L., Giunta, A. A., Grossman, B., Haftka, R. T., Mason, W. H., and Watson, L. T., "Variable-Complexity Response Surface Approximations for Wing Structural Weight in HSCT Design," *Computational Mechanics*, 18(2), pp. 112–126, 1996.
5. Knill, D. L., Giunta, A. A., Baker, C. A., Grossman, B., Mason, W. H., Haftka, R. T., and Watson, L. T., "Multidisciplinary HSCT Design using Response Surface Approximations of Supersonic Euler Aerodynamics," AIAA 98–0905, *36th Aerospace Sciences Meeting and Exhibit*, Reno, NV, January 1998.
6. Mason, B. H., Haftka, R. T., and Johnson, E. R., "Analysis and Design of Composite Channel Frames," AIAA Paper 94–4364–CP, Proceedings of the *5th AIAA/NASA/USAF/ISSMO Symposium on Multidisciplinary Analysis and Optimization*, Panama City, Florida, Sept. 7–9, 1994, Vol. 2, pp. 1023–1040.
7. Vitali, R, Haftka, R. T., and Sankar, B. V., "Response Surface Approximations for Crack Propagation Critical Loads," AIAA Paper 98–2047, Proceedings, *39th AIAA/ASME/ASCE/AHS/ASC Structures, Structural Dynamics, and Materials Conference*, Long Beach, California, April 20–23, 1998, Vol. 4., pp. 2917–2922.

8. Carlson, Harry W. and Walkley, Kenneth B., "Numerical Methods and a Computer Program for Subsonic and Supersonic Aerodynamic Design and Analysis of Wings With Attainable Thrust Corrections," NASA CP 3808, 1984.
9. Torenbeek, E., "Development and Application of a Comprehensive, Design-Sensitive Weight Prediction Method for Wing Structures of Transport Category Aircraft," Delft University of Technology, September 1992, Report LR–693.
10. Scott, P. W., "Developing Highly Accurate Empirical Weight Estimation Relationships: Obstacles and Tactics," Proceedings of the *51st International Conference of the Society of Weight Engineers*, May 1992, SAWE Paper No. 2091.
11. McCullers, L. A., "Aircraft Configuration Optimization Including Optimize Flight Profiles," Proceedings of a *Symposium on Recent Experiences in Multidisciplinary Analysis and Optimization*, April 1984, pp. 395–412, J. Sobieski, compiler, NASA CP–2327.
12. Huang, X., Dudley, J., Haftka, R. T., Grossman, B., and Mason, W., "Structural Weight Estimation for Multidisciplinary Optimization of a High-Speed Civil Transport", *Journal of Aircraf*, Vol. 33, No. 3, pp. 608–616, 1996.
13. Barthelemy, J. F. M., Wrenn, G. A., Dovi A. R., Coen, P. G., and Hall, L. E., "Supersonic Transport Wing Minimum Weight Design Integrating Aerodynamics and Structures," *Journal of Aircraft*, Vol. 31, No. 2, pp. 330–338, March–April 1994.
14. Balabanov, V., Kaufman, M., Knill, D. L, Haim, D., Golovidov, O., Giunta, A. A., Haftka, R. T., Grossman, B., Mason, W. H., and Watson, L. T., "Dependence of Optimal Structural Weight on Aerodynamic Shape for a High-Speed Civil Transport," AIAA Paper 96-4046, Proceedings of the *6th AIAA/NASA/USAF/ISSMO Symposium on Multidisciplinary Analysis and Optimization*, Bellevue, WA, Sept. 4–6, 1996, pp. 599–612.
15. Balabanov, V., "Development of Approximations for HSCT Wing Bending Material Weight using Response Surface Methodology," Ph.D. dissertation, Virginia Polytechnic Institute and State University, September, 1997.
16. VMA Engineering, 1767 S. 8th Street, Suite M–200, Colorado Springs, CO 80906, GENESIS User Manual, Version 4.0, October 1997.
17. SAS Institute, Inc., SAS Campus Drive, Cary, NC 27513, SAS Users Guide, Version 6, Fourth Edition, 1990.
18. Myers, R. H. and Montgomery, D. C., "*Response Surface Methodology. Process and Product Optimization Using Designed Experiments*," John Wiley and Sons, Inc., New York, N. Y., 1995.
19. Giunta, A. A., Balabanov, V., Haim, D., Grossman, B., Mason, W. H., Watson, L. T., and Haftka, R. T., "Multidisciplinary Optimization of a Supersonic Transport Using Design of Experiments Theory and Response Surface Modeling", *Aeronautical Journal*, Vol. 101, No. 1008, pp. 489–494, October 1997.